Time-domain Dynamic State Estimation for Unbalanced Three-phase Power Systems

Martin Pfeifer, Felicitas Mueller, Steven de Jongh, Frederik Gielnik, Thomas Leibfried, and Sören Hohmann

Abstract—In this paper, we present a time-domain dynamic state estimation for unbalanced three-phase power systems. The dynamic nature of the estimator stems from an explicit consideration of the electromagnetic dynamics of the network, i.e., the dynamics of the electrical lines. This enables our approach to release the assumption of the network being in quasi-steady state. Initially, based on the line dynamics, we derive a graph-based dynamic system model. To handle the large number of interacting variables, we propose a port-Hamiltonian modeling approach. Based on the port-Hamiltonian model, we then follow an observer-based approach to develop a dynamic estimator. The estimator uses synchronized sampled value measurements to calculate asymptotic convergent estimates for the unknown bus voltages and currents. The design and implementation of the estimator are illustrated through the IEEE 33-bus system. Numerical simulations verify the estimator to produce asymptotic exact estimates, which are able to detect harmonic distortion and sub-second transients as arising from converter-based resources.

Index Terms—Dynamic state estimation, power system, harmonic, observer, port-Hamiltonian system, static state estimation, transient.

I. INTRODUCTION

STATE estimation techniques are inevitable for power system monitoring, control, and protection. Nowadays, the state estimation in power system control centers is realized in form of a weighted least squares (WLS) estimation [1], [2]. The core of this WLS approach dates back to [3] and is based on the assumption that the system is in quasi-steady state. Indeed, this assumption was justified at earlier time. However, in recent years, power systems have experienced a tremendous extension of converter-based resources such as wind and solar power renewable generation, energy storages, and power electronic loads. With the increasing penetration

of these converter-based resources, the system dynamic responses are heavily dependent on the fast-response power electronic devices and their controls. In consequence, converter-induced dynamics and stability issues on a sub-second time scale start to dominate the system [4]-[6]. This makes the quasi-steady state assumption and therewith a WLS-based state estimation inadmissible [1], [7]. In particular, the existing WLS-based protection functions may become inadequate [7].

Due to these reasons, new sub-second state estimation tools are required for monitoring, control, and protection of power systems. Power system dynamic state estimation (DSE) is a promising approach to provide such tools. DSE approaches are based on a dynamic model of the power system and fast-sampled and time-synchronized measurements. In the sequel, we distinguish between two different classes of DSE, viz. component-based DSE and network-based DSE.

In component-based DSE approaches, the dynamic states to be estimated are related to the components connected to the network, e.g., synchronous machines, storage systems, voltage source converters, or dynamic loads. Component-based DSE is a very active field of research as illustrated by the fruitful activities of the IEEE Task Force on Power System Dynamic State and Parameter Estimation [1], [7], [8]. Furthermore, the textbook in [9] outlines the fundamental idea of a DSE estimating the states of synchronous generators. Reference [10] presents a DSE based on an unknown input observer to estimate the dynamic states of reheater sections and storage systems. Another observer-based DSE approach can be found in the anomaly detection scheme from [11]. In [12], the unscented Kalman filter (UKF) is used to estimate the dynamic states of generators and power system stabilizers. Reference [13] extends this approach to asynchronous measurements. Reference [14] applies UKFs and particle filters to develop a DSE for the states of synchronous generators. An approach based on a sigma-point Kalman filter (SPKF) is presented in [15]. An unknown-input extended Kalman filter (EKF) is used in [16] for a robust estimation of the generator states. Other component-based DSE approaches based on an EKF have been proposed in [17]-[19]. Reference [20] presents a DSE which estimates the dynamic states of converter-interfaced generation units in microgrids.

A restriction of component-based DSE approaches is that they assume the network to be in quasi-steady state. As ar-

gued above, in converter-based power systems, this assumption is inadmissible leading to a blindness of component-based DSE approaches concerning important sub-second phenomena. This motivates a network-based DSE in which the dynamic states to be estimated are related to the variables from the network such as voltages and currents of buses and lines. Therewith, as with the classic WLS approach, the objective of a network-based DSE is to estimate the state of the network. However, network-based DSE has received limited attention in the literature. An exception is given by [21] in which the centralized and distributed DSEs for microgrids based on unknown-input Kalman filters are proposed. On the one hand, the estimators provide estimates of the dynamic states of components, viz. distributed generation units and capacitor banks. On the other hand, they provide estimates of the dynamic states of the network, viz. the lines in the *dq*-domain. However, to our knowledge, there are hardly no more reports into this direction. In other words, the benefit of considering the network dynamics for the state estimation has been largely unexplored.

In this paper, we bridge this research gap. To this end, we develop a time-domain dynamic model and state estimator for the sub-second time scale in unbalanced three-phase distribution systems. In both the model and the estimator, the dynamics stem from the electromagnetic phenomena of the electrical lines of the network. The dynamic states of components connected to the network (such as converters) are not explicitly considered in our approach. Naturally, due to the large number of lines in a power system, such an approach leads to a large number of interacting system variables in terms of inputs, states, and outputs. To deal with this complexity, we propose a port-Hamiltonian approach. Port-Hamiltonian system (PHS) is a powerful framework for modeling complex physical systems [22]. In particular, the port-Hamiltonian paradigm has a great affinity to graph theory. This makes this paradigm a promising framework for this paper as it is easily transferable to other configurations and well scalable to larger setups.

Based on the port-Hamiltonian approach, the contributions of this paper are threefold: ① a graph-based PHS model which explicitly considers the dynamics of the lines; ② a dynamic state estimator, which is based on the model from ① and can be designed offline in an automated manner; and ③ a simulation study in which we demonstrate that the state estimator from ② extends the functionalities of a WLS-based state estimation to a sub-second time scale.

Notation: vectors and matrices are written in bold font. Let $\boldsymbol{A} \in \mathbb{R}^{m \times n}$ be a matrix with m rows and n columns. For the transpose of $\boldsymbol{A}$, we write $\boldsymbol{A}^{\mathrm{T}}$. Let $\boldsymbol{B} \in \mathbb{R}^{p \times q}$. The Kronecker product of $\boldsymbol{A}$ and $\boldsymbol{B}$ is written as $\boldsymbol{A} \otimes \boldsymbol{B}$. Now let $m = n$. The inverse of $\boldsymbol{A}$ is denoted by $\boldsymbol{A}^{-1}$ (if it exists). $\boldsymbol{A} \succ 0$ means that $\boldsymbol{A}$ is positive-definite. The identity and zero matrices are denoted as $\boldsymbol{I}$ and $\boldsymbol{0}$, respectively. A block diagonal matrix of matrices is denoted by blkdiag(·).

Further, let $\mathbb{M}$ be a set of indices. For each $i \in \mathbb{M}$, suppose a variable $x_i \in \mathbb{R}$. For the vertical concatenation of all x_i in a vector $\boldsymbol{x}$, we write $\boldsymbol{x} = (x_i)$ and append "for all $i \in \mathbb{M}$".

Throughout this paper, the time-dependence "(t)" of variables and vectors is omitted in the notation.

The remainder of the paper is structured as follows. In Section II, we derive a graph-based PHS model of unbalanced three-phase systems. Based on the model, a dynamic state estimator is developed in Section III. In Section IV, the model generation and estimator design are exemplified for the IEEE 33-bus system. The estimation results are analyzed through numerical simulations. Section V concludes the paper and outlines directions for future research.

II. System Modeling

A. System Description

Consider an unbalanced three-phase power system with N buses. The three phases are collected in the set $\mathbb{P} = \{A, B, C\}$. P of the N buses are connected to higher-level systems. The remaining $N - P$ buses are connected to $N - P$ loads. Distributed power generation is described by a negative load. The N buses are connected by M three-phase lines. The topology of the power system is described by a connected graph $\mathcal{G} = (\mathbb{V}, \mathbb{E})$, where $\mathbb{V}$ and $\mathbb{E}$ contain N buses and M lines, respectively.

Figure 1 shows an exemplary system with $N = 33$, $M = 32$, and $P = 1$. The depicted system is the well-known IEEE 33-bus system from [23]. The nominal voltage of this system is 12.66 kV, and the system frequency is 50 Hz.
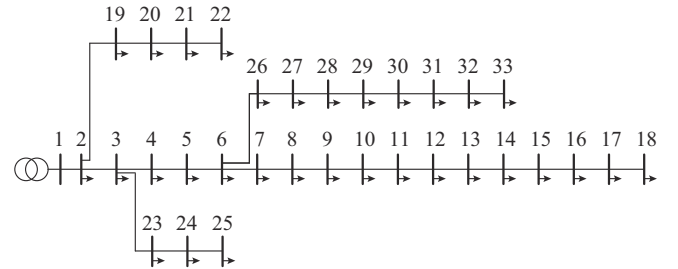
Fig. 1. Schematic diagram of IEEE 33-bus system.

B. Line Model

A line $j \in \mathbb{E}$ is described by the π-section model in Fig. 2. The π-section model considers phase resistances $R_{k,j}$, phase self inductances $L_{k,k,j}$ and phase-phase mutual inductances $L_{k,l,j}$, where $k, l \in \mathbb{P}$, $k \neq l$. The mutual inductances are necessary to consider lines that are untransposed [24]. Shunt elements are neglected, which is permissible in the majority of systems [24]. The resistances and inductances are collected in the following resistance and inductance matrices, respectively, with $\boldsymbol{R}_j = \boldsymbol{R}_j^{\mathrm{T}} \succ 0$, $\boldsymbol{L}_j = \boldsymbol{L}_j^{\mathrm{T}} \succ 0$ for all $j \in \mathbb{E}$.

$$\boldsymbol{R}_j = \begin{bmatrix} R_{A,j} & 0 & 0 \\ 0 & R_{B,j} & 0 \\ 0 & 0 & R_{C,j} \end{bmatrix} \tag{1a}$$

$$\boldsymbol{L}_j = \begin{bmatrix} L_{A,A,j} & L_{A,B,j} & L_{A,C,j} \\ L_{A,B,j} & L_{B,B,j} & L_{B,C,j} \\ L_{A,C,j} & L_{B,C,j} & L_{C,C,j} \end{bmatrix} \tag{1b}$$
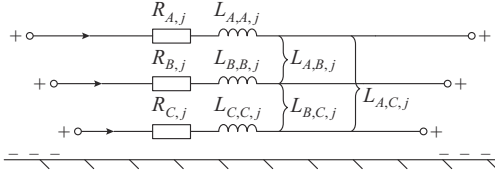
Fig. 2. π-section equivalent circuit of a three-phase line.

C. Power System Model

Based on the line model from the previous subsection, we now derive a graph-based model of the power system. We consider an unbalanced system whose topology is described by the directed graph $\mathcal{G} = (\mathbb{V}, \mathbb{E})$ with the incidence matrix $\boldsymbol{B}$.

First, we define the vectors of all bus voltages and bus currents as $\boldsymbol{v}^{\mathrm{bus}} := \left(v_{i,j}^{\mathrm{bus}} \right) \in \mathbb{R}^{3N}$ and $\boldsymbol{i}^{\mathrm{bus}} := \left(i_{i,j}^{\mathrm{bus}} \right) \in \mathbb{R}^{3N}$, respectively, for all $i \in \mathbb{P}$ and $j \in \mathbb{V}$. With "bus current", we refer either to a current between a bus and a source of supply (e.g., bus 1 in Fig. 1) or to a current between a bus and a load (e.g., buses 2 to 33 in Fig. 1). Likewise, the vector of voltages across lines and the vector of currents through lines are defined as $\boldsymbol{v}^{\mathrm{line}} := \left(v_{i,j}^{\mathrm{line}} \right) \in \mathbb{R}^{3M}$ and $\boldsymbol{i}^{\mathrm{line}} := \left(i_{i,j}^{\mathrm{line}} \right) \in \mathbb{R}^{3M}$, respectively, for all $i \in \mathbb{P}$ and $j \in \mathbb{E}$. Moreover, we define the vector of all magnetic flux linkages of the line inductances as $\boldsymbol{\psi}^{\mathrm{line}} := \left(\psi_{i,j}^{\mathrm{line}} \right) \in \mathbb{R}^{3M}$ for all $i \in \mathbb{P}$ and $j \in \mathbb{E}$.

From the law of inductance, the voltages across the line inductances are given by:

$$\boldsymbol{v}^{\mathrm{ind}} = \dot{\boldsymbol{\psi}} \qquad (2)$$

The currents through the inductances (and therewith the line currents) can be expressed as:

$$\boldsymbol{v}^{\mathrm{ind}} = \boldsymbol{i}^{\mathrm{line}} = \frac{\partial \boldsymbol{H}}{\partial \boldsymbol{\psi}} \qquad (3)$$

In (3), the function $\boldsymbol{H}$ describes the energy contained in the line inductances and is given by (4) with $\boldsymbol{Q} = \mathrm{blkdiag}\left(\boldsymbol{L}_j^{-1} \right)$, where the matrix $\boldsymbol{L}_j$ is from (2) for $j \in \mathbb{E}$. Note that by the symmetry and positive definiteness of $\boldsymbol{L}_j$, we have $\boldsymbol{Q} = \boldsymbol{Q}^{\mathrm{T}} \succ 0$.

$$\boldsymbol{H} = \frac{1}{2} \boldsymbol{\psi}^{\mathrm{T}} \boldsymbol{Q} \boldsymbol{\psi} \qquad (4)$$

By Kirchhoff's voltage law, the line voltages and the bus voltages are related in terms of:

$$\boldsymbol{v}^{\mathrm{line}} = -\left(\boldsymbol{B} \otimes \boldsymbol{I}_3 \right)^{\mathrm{T}} \boldsymbol{v}^{\mathrm{bus}} \qquad (5)$$

where $\boldsymbol{I}_3$ is the 3×3 identity matrix.

The bus and line currents satisfy Kirchhoff's current law:

$$\boldsymbol{i}^{\mathrm{bus}} = -\left(\boldsymbol{B} \otimes \boldsymbol{I}_3 \right) \boldsymbol{i}^{\mathrm{line}} \qquad (6)$$

The voltage drop across the lines is composed of the voltage drop across the line resistances $\boldsymbol{v}^{\mathrm{line}}$ and the voltage drop across the line inductances $\boldsymbol{v}^{\mathrm{ind}}$ (cf. Fig. 2):

$$\boldsymbol{v}^{\mathrm{line}} = \boldsymbol{v}^{\mathrm{ind}} + \boldsymbol{v}^{\mathrm{res}} \qquad (7)$$

The voltage drop across the line resistances is given by:

$$\boldsymbol{v}^{\mathrm{res}} = \boldsymbol{R} \boldsymbol{i}^{\mathrm{line}} \qquad (8)$$

where $\boldsymbol{R} = \mathrm{blkdiag}\left(\boldsymbol{R}_j \right)$ with $\boldsymbol{R}_j$ from (1) for $j \in \mathbb{E}$. By inserting (5) and (8) into (7), we can obtain:

$$\boldsymbol{v}^{\mathrm{ind}} = -\boldsymbol{R} \boldsymbol{i}^{\mathrm{line}} - \left(\boldsymbol{B} \otimes \boldsymbol{I}_3 \right)^{\mathrm{T}} \boldsymbol{v}^{\mathrm{bus}} \qquad (9)$$

By inserting (2) and (3) into (9) and (6), we then obtain the dynamic model with $\boldsymbol{G} = -\left(\boldsymbol{B} \otimes \boldsymbol{I}_3 \right)^{\mathrm{T}}$ and $\boldsymbol{H}$ from (4).

The model (10) is a state-space model in form of an explicit PHSs (cf. [22]). Therewith, (10) is a purely physical model describing the relations between the system variables. In particular, $\boldsymbol{i}^{\mathrm{bus}} = \boldsymbol{G}^{\mathrm{T}} \partial \boldsymbol{H} / \partial \boldsymbol{\psi}$ generally does not coincide with the system measurement equation. In the next subsection, we thus extend the model (10) by a model of the measurements.

$$\boldsymbol{\psi} = -\boldsymbol{R} \frac{\partial \boldsymbol{H}}{\partial \boldsymbol{\psi}} + \boldsymbol{G} \boldsymbol{v}^{\mathrm{bus}} \qquad (10a)$$

$$\boldsymbol{i}^{\mathrm{bus}} = \boldsymbol{G}^{\mathrm{T}} \frac{\partial \boldsymbol{H}}{\partial \boldsymbol{\psi}} \qquad (10b)$$

D. Measurement Model

We consider synchronized sampled value measurements (cf. [7]) of voltages and currents at subsets $\mathbb{V}_v^{\mathrm{M}}$ and $\mathbb{V}_i^{\mathrm{M}}$ of the set of buses $\mathbb{V}$, respectively, i.e., $\mathbb{V}_v^{\mathrm{M}}, \mathbb{V}_i^{\mathrm{M}} \subseteq \mathbb{V}$. The linear independent voltage measurements at the subset $\mathbb{V}_v^{\mathrm{M}}$ are described by a voltage measurement vector $\boldsymbol{m}_v \in \mathbb{R}^{q_v}$ with $q_v < 3N$.

$$\boldsymbol{m}_v = \boldsymbol{M}_v \boldsymbol{v}^{\mathrm{bus}} \qquad (11)$$

The matrix $\boldsymbol{M}_v \in \{0, 1\}^{q_v \times 3N}$ is a selector matrix that determines which of the bus voltages are measured. In a selector matrix, each row is a transposed unit vector [25].

$$\bar{\boldsymbol{m}}_v = \bar{\boldsymbol{M}}_v \boldsymbol{v}^{\mathrm{bus}} \qquad (12)$$

where $\bar{\boldsymbol{M}}_v$ is the complimentary matrix to $\boldsymbol{M}_v$, i.e., a selector matrix which picks the unmeasured bus voltages from the vector of all bus voltages. Note that by the properties of $\boldsymbol{M}_v$ and $\bar{\boldsymbol{M}}_v$, the composite matrix $\left[\boldsymbol{M}_v^{\mathrm{T}}, \bar{\boldsymbol{M}}_v^{\mathrm{T}} \right]^{\mathrm{T}}$ is a permutation matrix and therewith orthogonal.

The current measurements $\boldsymbol{m}_i \in \mathbb{R}^{q_i}$ at the subset $\mathbb{V}_i^{\mathrm{M}}$ can be described by:

$$\boldsymbol{m}_i = \boldsymbol{M}_i \boldsymbol{i}^{\mathrm{bus}} \qquad (13)$$

where $\boldsymbol{M}_i \in \{0, \pm 1\}^{q_i \times 3N}$ and $q_i < 3(N+M)$.

E. Model Discussion

The PHS (10) is a graph-based model of three-phase power systems. For a particular system, one obtains the particular system model by specifying the number of buses N, the number of lines M, the (directed) incidence matrix $\boldsymbol{B}$, and the resistance and inductance matrices in (1). Thereby, we can assign the resistance and inductance values individually to each of the three phases of each line, making the model capable of describing unbalanced power systems.

The dynamic states of the model (10) are the magnetic flux linkages of the self and mutual inductances of the three-phase lines. The inputs and outputs of the model are given by the bus voltages and bus currents, respectively. The bus currents are used to describe loads and generation units in terms of current extractions and injections, respectively.

Note that with the bus voltages and bus currents, we can calculate all other voltages and currents in the power system.

The model (10) is defined in the time domain on a sub-second time scale. Hence, in the nominal case, the time courses of the model variables are oscillating with the system frequency (e.g., 50 Hz or 60 Hz).

The measurement model consists of two parts, viz. the voltage measurement equation (11) and the current measurement equation (13). The voltage measurement equation describes which of the bus voltages are being measured. The current measurement equation may describe the measurements of bus currents and line currents (expressed through bus currents). The basis for the validity of the measurement models (11) and (13) is fast-sampled and time-synchronized sampled value measurements [7]. Phasor measurement units (PMUs) provide such measurements with a high signal-to-noise ratio (SNR) and typical sampling times between 0.15 and 0.2 [26].

Based on model (10) and the measurement models (11) and (13), the next section is devoted to the development of an estimator for unbalanced three-phase power systems.

III. ESTIMATOR DESIGN

A. Dynamic Estimator

Consider the system model in (10) with voltage measurements (11) and current measurements (13).

By inserting (4) into (10a) and using the orthogonality of $\left[\boldsymbol{M}_v^{\mathrm{T}}, \bar{\boldsymbol{M}}_v^{\mathrm{T}} \right]^{\mathrm{T}}$, the dynamics equation can be rewritten as:

$$\dot{\boldsymbol{\psi}} \overset{(4)}{=} -\boldsymbol{RQ\psi} + \boldsymbol{G} \begin{bmatrix} \boldsymbol{M}_v^{\mathrm{T}} & \bar{\boldsymbol{M}}_v^{\mathrm{T}} \end{bmatrix} \begin{bmatrix} \boldsymbol{M}_v \\ \bar{\boldsymbol{M}}_v \end{bmatrix} \boldsymbol{v}^{\mathrm{bus}} \overset{(11),\,(12)}{=}$$

$$-\boldsymbol{RQ\psi} + \boldsymbol{G} \begin{bmatrix} \boldsymbol{M}_v^{\mathrm{T}} & \bar{\boldsymbol{M}}_v^{\mathrm{T}} \end{bmatrix} \begin{bmatrix} \boldsymbol{m}_v \\ \bar{\boldsymbol{m}}_v \end{bmatrix} = -\boldsymbol{RQ\psi} + \boldsymbol{GM}_v^{\mathrm{T}} \boldsymbol{m}_v + \boldsymbol{G\bar{M}}_v^{\mathrm{T}} \bar{\boldsymbol{m}}_v \tag{14}$$

Moreover, by inserting (10b) into (13), we can obtain:

$$\boldsymbol{m}_i = \boldsymbol{M}_i \boldsymbol{G}^{\mathrm{T}} \boldsymbol{Q\psi} =: \boldsymbol{C\psi} \tag{15}$$

Based on the dynamics equation (14) and the measurements (15), we now derive a dynamic estimator. Note that in (14), the states (i.e., the magnetic flux linkages of the lines) are unknown as they are not measured during system operation. Moreover, with $\bar{\boldsymbol{m}}_v$, (14) contains unknown inputs. In the sequel, we address this setup with an unknown input observer (note that by discretizing (14), we could also approach with a Kalman filter). In order to ensure the existence of such an observer, we make the following assumption.

Assumption 1: the system in (14) and (15) is strong* detectable.

Appendix A provides a brief introduction into the concept of strong* detectability. The existence condition from Assumption 1 now allows to state the main theorem of this section. In this theorem, we propose an estimator for the unknown system variables.

Theorem 1: for the dynamic system consisting of (14) and (15), let Assumption 1 hold. Then, there exist matrices $\boldsymbol{N} \in \mathbb{R}^{3M \times 3M}$, $\boldsymbol{L} \in \mathbb{R}^{3M \times q_i}$, $\boldsymbol{F} \in \mathbb{R}^{3M \times q_v}$, and $\boldsymbol{E} \in \mathbb{R}^{3M \times q_i}$, such that

the system of (16) yields estimates $\hat{\boldsymbol{\psi}}$, $\hat{\bar{\boldsymbol{m}}}_v$, and $\hat{\boldsymbol{i}}^{\mathrm{bus}}$, which asymptotically converge towards the unknown flux linkages $\boldsymbol{\psi}$, the unmeasured bus voltages $\bar{\boldsymbol{m}}_v$, and the bus currents $\boldsymbol{i}^{\mathrm{bus}}$, respectively. In (16), the vector $\boldsymbol{z} \in \mathbb{R}^{3M}$ is the estimator state and the term $\left(\boldsymbol{CG\bar{M}}_v^{\mathrm{T}} \right)^{+}$ is the Moore-Penrose inverse of $\boldsymbol{CG\bar{M}}_v^{\mathrm{T}}$.

$$\dot{\boldsymbol{z}} = \boldsymbol{Nz} + \boldsymbol{Lm}_i + \boldsymbol{Fm}_v \quad \boldsymbol{z}\big|_{t=0} = \boldsymbol{z}_0 \tag{16a}$$

$$\hat{\boldsymbol{\psi}} = \boldsymbol{z} - \boldsymbol{Em}_i \tag{16b}$$

$$\hat{\bar{\boldsymbol{m}}}_v = \left(\boldsymbol{CG\bar{M}}_v^{\mathrm{T}} \right)^{+} \left(\dot{\boldsymbol{m}}_i + \boldsymbol{CRQ\hat{\psi}} - \boldsymbol{CGM}_v^{\mathrm{T}} \boldsymbol{m}_v \right) \tag{16c}$$

$$\hat{\boldsymbol{i}}^{\mathrm{bus}} = \boldsymbol{G}^{\mathrm{T}} \boldsymbol{Q\hat{\psi}} \tag{16d}$$

Proof: we first verify that (16a) and (16b) yield an asymptotically converging estimate of the flux linkages—independently of the unknown bus voltages. To this end, we apply the unknown-input observer from [27]. Afterwards, we show that (16c) and (16d) yield asymptotically converging estimates of the unknown bus voltages and bus currents, respectively.

Let Assumption 1 hold. Consider the estimation error $\boldsymbol{\varepsilon} = \hat{\boldsymbol{\psi}} - \boldsymbol{\psi}$. The dynamics of the estimation error read:

$$\dot{\boldsymbol{\varepsilon}} = \dot{\hat{\boldsymbol{\psi}}} - \dot{\boldsymbol{\psi}} \overset{(14),\,(16b)}{=} \dot{\boldsymbol{z}} - \boldsymbol{E\dot{m}}_i - \left(-\boldsymbol{RQ\psi} + \boldsymbol{Gm}_v + \boldsymbol{G\bar{M}}_v^{\mathrm{T}} \bar{\boldsymbol{m}}_v \right) \overset{(16a),\,(16b)}{=}$$

$$\boldsymbol{N}\left(\hat{\boldsymbol{\psi}} + \boldsymbol{Em}_i \right) + \boldsymbol{Lm}_i + \boldsymbol{Fm}_v - \boldsymbol{E\dot{m}}_i + \boldsymbol{RQ\psi} -$$

$$\boldsymbol{GM}_v^{\mathrm{T}} \boldsymbol{m}_v - \boldsymbol{G\bar{M}}_v^{\mathrm{T}} \bar{\boldsymbol{m}}_v \overset{(14),\,(15)}{=} \boldsymbol{N\varepsilon} + \left(\boldsymbol{NK} + \boldsymbol{LC} + \boldsymbol{KRQ} \right) \boldsymbol{\psi} +$$

$$\left(\boldsymbol{F} - \boldsymbol{KGM}_v^{\mathrm{T}} \right) \boldsymbol{m}_v - \boldsymbol{KGM}_v^{\mathrm{T}} \boldsymbol{m}_v \tag{17}$$

where $\boldsymbol{K} = \boldsymbol{I} + \boldsymbol{EC}$. Suppose we have:

$$0 = \boldsymbol{NK} + \boldsymbol{LC} + \boldsymbol{KRQ} \tag{18a}$$

$$0 = \boldsymbol{F} - \boldsymbol{KGM}_v^{\mathrm{T}} \tag{18b}$$

$$0 = \boldsymbol{KGM}_v^{\mathrm{T}} \tag{18c}$$

If the conditions in (18) hold, (17) reads $\dot{\boldsymbol{\varepsilon}} = \boldsymbol{N\varepsilon}$. If, in addition, $\boldsymbol{N}$ is a Hurwitz matrix, we have $\boldsymbol{\varepsilon} \to 0$ for $t \to \infty$. Next, we show that we can always find matrices $\boldsymbol{N}$, $\boldsymbol{L}$, $\boldsymbol{F}$, and $\boldsymbol{E}$ such that the conditions in (18) are fulfilled and $\boldsymbol{N}$ is a Hurwitz matrix.

Assumption 1 implies $rank\left(\boldsymbol{CG\bar{M}}_v^{\mathrm{T}} \right) = rank\left(\boldsymbol{G\bar{M}}_v^{\mathrm{T}} \right) = 3N - q_v$ [28]. Hence, from (18c), we obtain the solution set for $\boldsymbol{E}$ with $\left(\boldsymbol{CGM}_v^{\mathrm{T}} \right)^{+} = \left(\left(\boldsymbol{CGM}_v^{\mathrm{T}} \right)^{\mathrm{T}} \left(\boldsymbol{CGM}_v^{\mathrm{T}} \right) \right)^{-1} \left(\boldsymbol{CGM}_v^{\mathrm{T}} \right)^{\mathrm{T}}$ and $\boldsymbol{Y} \in \mathbb{R}^{3N \times (3N - q_v)}$ as an arbitrary matrix.

$$\boldsymbol{E} = -\boldsymbol{GM}_v^{\mathrm{T}} \left(\boldsymbol{CGM}_v^{\mathrm{T}} \right)^{+} + \boldsymbol{Y} \left(\boldsymbol{I} - \left(\boldsymbol{CGM}_v^{\mathrm{T}} \right) \left(\boldsymbol{CGM}_v^{\mathrm{T}} \right)^{+} \right) \tag{19}$$

Based on a particular solution for $\boldsymbol{E}$, we can calculate $\boldsymbol{F}$ from (18b):

$$\boldsymbol{F} = \left(\boldsymbol{I} + \boldsymbol{EC} \right) \boldsymbol{GM}_v^{\mathrm{T}} \tag{20}$$

For the determination of the matrix $\boldsymbol{N}$, we rewrite (18a) as:

$$\boldsymbol{N} = -\boldsymbol{KRQ} - \boldsymbol{ZC} \tag{21}$$

where $\boldsymbol{Z} = \boldsymbol{L} + \boldsymbol{NE}$. From [27] and [28], it follows that Assumption 1 implies the pair $\left(-\boldsymbol{KRQ}, \boldsymbol{C} \right)$ to be detectable. Thus, there always exists a matrix $\boldsymbol{Z}$ such that $\boldsymbol{N}$ is Hurwitz. Substituting (21) into $\boldsymbol{Z} = \left(\boldsymbol{L} + \boldsymbol{NE} \right)$ yields the following expression for $\boldsymbol{L}$, which then satisfies (18a).

$$L = Z(I + CE) + KRQE \qquad (22)$$

Hence, we can always find matrices (N, L, F, E) such that the conditions in (18) are satisfied and such that N is a Hurwitz matrix.

For the estimation of the unknown bus voltages, we derive (15) with respect to time:

$$\dot{m}_i = C\dot{\psi} = -CRQ\psi + CGM_v^T m_v + CG\bar{M}_v^T \bar{m}_v \qquad (23)$$

With $\left(CGM_v^T\right)^+$, we may solve (23) for $\bar{m}_v$:

$$\bar{m}_v = \left(CG\bar{M}_v^T\right)^+ \left(\dot{m}_i + CRQ\psi - CGM_v^T m_v\right) \qquad (24)$$

In (24), we substitute $\bar{m}_v$ with $\hat{\bar{m}}_v$ and ψ with $\hat{\psi}$ and obtain (16c). By comparing (24) and (16c), we may deduce $\hat{\bar{m}}_v \to \bar{m}_v$ from $\hat{\psi} \to \psi$ for $t \to \infty$. Finally, from (10b), (16d), and $\hat{\psi} \to \psi$, we may directly infer $\hat{i}^{\text{bus}} \to i^{\text{bus}}$ for $t \to \infty$.

B. Estimator Discussion

The dynamic estimator (16) produces asymptotically converging estimates of the unknown bus voltages, the bus currents, and flux linkages based on the measurements m_v and m_i. As a model, the estimator is able to reconstruct system imbalances, sub-second transients, and harmonic distortion. Therewith, the dynamic estimator extends the functionalities of a classical WLS-based state estimation for advanced power system monitoring, control and protection schemes [7]. As with the WLS-based state estimation, the estimator (16) focuses only on the network states; and the states of components connected to the network such as converters and synchronous generators are not estimated.

Note that (16) denotes a linear state-space system which can be solved numerically by using well-known techniques such as Euler or Runge-Kutta methods. Equation (16c) requires the first time-derivative of the current measurements. Reference [29] shows that a time-derivative of the measurement vector is unavoidable if one aims for a reconstruction of the unknown inputs. This suggests that the estimator (16) is vulnerable to measurement noise. In Section IV, we will analyze this vulnerability in detail via numerical simulations.

It is noteworthy that the matrices N, L, F, and E for the estimator (16) can be computed in an automated manner. Algorithm 1 provides a pseudocode listing to compute these matrices. For the evaluation of Assumption 1, there exist simple algebraic criteria for which the reader is referred to [27] and [28]. Hence, the design of the estimator (16) is fully automatable and can be conducted offline. Moreover, the online execution of the estimator requires a small number of matrix multiplications and thus involves little computational costs.

Algorithm 1: automated design of the estimator of (16)

Input: model (10) with measurements (11) and (13)

1: Set up (14) and (15)

2: Calculate E and F from (19) and (20), respectively

3: Specify the eigenvalues of N

4: Calculate Z from (21) by pole placement techniques

5: Calculate N and L from (21) and (22), respectively

6: **Return** (N, L, F, E)

IV. SIMULATION STUDY

In this section, we illustrate the model (10) and the estimator (16) for the IEEE 33-bus system from Fig. 1. The particular aims of the study are: ① to evaluate the validity of the model and the estimator; and ② to compare the performance of the estimator with the performance of a WLS-based estimation of the network variables. Note that a comparison between the estimator (16) and DSE methods from the literature is not possible. Our approach differs from the existing approaches in the states to be estimated as well as in the measurement and model information underlying the estimation (cf. Section I).

A. Model Derivation and Estimator Design

The IEEE 33-bus system from Fig. 1 contains $N = 33$ buses and $M = 32$ lines. The incidence matrix B describes the topology of the system. The numeric values of the resistance and inductance matrices in (1) are taken from [23].

By inserting the incidence matrix, the resistance matrices, and the inductance matrices into (10), we obtain a dynamic model of the IEEE 33-bus system. The state vector, the input vector, and the output vector of the model are given by the flux linkages $\psi \in \mathbb{R}^{96}$, the bus voltages $v^{\text{bus}} \in \mathbb{R}^{99}$, and the bus currents $i^{\text{bus}} \in \mathbb{R}^{99}$, respectively.

To demonstrate the estimator design, we first define the sets of current and voltage measurement buses $\mathbb{V}_i^M$ and $\mathbb{V}_v^M$, respectively. We assume the following buses to be equipped with current measurements: $\mathbb{V}_i^M = \{2, 4, 6, 8, 10, 12, 14, 16, 18, 20, 22, 23, 25, 27, 29, 31, 33\}$. In each measurement bus $i \in \mathbb{V}_i^M$, sensors provide synchronized sampled value measurement of the three-phase line currents, i.e., the currents flowing through the incident lines. The bus currents are assumed to be nonmeasured. The current measurements are collected in the measurement vector $m_i \in \mathbb{R}^{96}$. The dimension of 96 is calculated from 3×32, where "3" accounts for three-phase measurements and "32" for the number of lines being incident to the buses from $\mathbb{V}_i^M$. From the relation between the line currents and the bus currents in (6), we may then formulate a measurement equation in the form (13).

For the entire system, we assume only one three-phase bus voltage measurement which is located at bus 2, i.e., $\mathbb{V}_v^M = \{2\}$. This voltage measurement acts as a reference for the voltage estimates and constitutes the voltage measurement vector $m_v \in \mathbb{R}^3$. From this, we can directly formulate a measurement equation (11).

Based on the two measurement equations (11) and (13) and the dynamic model (10), we apply Algorithm 1 to compute an estimator of the form (16). In the obtained estimator, $\psi \in \mathbb{R}^{96}$, $m_v \in \mathbb{R}^{96}$, and $i^{\text{bus}} \in \mathbb{R}^{99}$ are estimates of the unknown flux linkages, the unmeasured bus voltages, and the unmeasured bus currents, respectively. The matrix N is calculated as a diagonal matrix with negative entries. The matrix E is a sparse matrix in which the arrangement of the non-zero matrix blocks reflects the structure of the incidence matrix of the graph $\mathcal{G} = (\mathbb{V}, \mathbb{E})$. The matrices L and F are calculated to be zero.

B. Simulation Setup

In this subsection, the model and estimator obtained in Section IV-A are analyzed through numerical simulations. As a ground truth, we use the MATLAB/Simulink time-domain simulation model of the IEEE 33-bus system from [30]. By default, this simulation model describes a scenario in which the system is balanced and in quasi-steady state. Hence, to account for the recent changes in power systems, the model from [30] is modified in three points.

1) On buses $\{4, 21, 27, 30, 31\}$, $\{7, 17, 22, 25, 26\}$, and $\{3, 12, 24, 28, 32\}$, load imbalances for the phases A, B, and C are introduced, respectively. For these buses, the load at the concerning phase is 30 higher than the load at the other two phases.

2) At $t_1 = 1$, $t_2 = 2$, and $t_3 = 3$, we consider load transients in which the active and reactive power of the three-phase loads at buses 14, 17, and 26, respectively, increase by the factor 2.

3) The voltage at bus 1 is subject to harmonic distortion. We consider the 3rd, 5th, 7th and 11th harmonics of the system frequency (i.e., 50 Hz). The amplitudes of the harmonics are set to be 2.5% of the amplitude of the system frequency. This yields a total harmonic distortion of 5, which is within the range of an allowed total harmonic distortion [31].

From now on, we denote the modified model from [30] as ground truth model.

For the evaluation of the model and estimator, first, the ground truth model has been simulated which results in time series for all bus voltages, bus currents, line currents, and line flux linkages. Moreover, we obtain time series for all variables from the vectors $\boldsymbol{m}_v$ and $\boldsymbol{m}_i$. The bus voltages constitute the input vector of the model (10). Hence, based on the time series of the bus voltages, we simulate (10). The output of this simulation is, amongst others, the time series for the bus currents (i.e., the output vector of (10)). Likewise, with the time series for $\boldsymbol{m}_v$ and $\boldsymbol{m}_i$, we simulate the estimator (16) and obtain time-series for the estimates of the unmeasured bus voltages and currents.

In order to compare the results of the estimator (16) with the results obtained from a WLS estimation, we design a standard three-phase unbalanced WLS estimator. Thereby, we consider the same measured variables as for the estimator (16). To simulate the WLS estimator, the time series of the variables from the vectors $\boldsymbol{m}_v$ and $\boldsymbol{m}_i$ from the ground truth model are transferred to the phasor domain by phase-locked loops (PLLs). The parametrization of the PLLs is conducted via the advanced tuning method from [32] with window length $T_w = 0.01$, design parameter $b = 2.4$, nominal voltage $v_N = 12.66$ kV, and nominal current $i_N = 10$ A. To enable a comparison between the WLS estimator and the estimator (16), the estimates obtained from the WLS estimator are re-transferred to the time domain by converting the phasors into sine signals with the corresponding phases and amplitudes.

All simulations were run with the same resolution on a computer with Intel$^{\text{(R)}}$ Core$^{\text{(TM)}}$ i7-6600U CPU @ 2.60 GHz and 12 GB RAM in MATLAB/Simulink R2019a with a fixed-step solver at a simulation step size of 0.01 ms. The initial values are chosen such that the simulations start in quasi-steady state. The simulation time horizon is $T = 4$ s.

C. Simulation Results

For the evaluation of the model (10) and estimator (16), we use the relative error signal power (RESP). Note that the deterministic and periodic nature of the signals obtained from the model (1) and estimator (2) makes the well-known similarity measures from statistics inappropriate for this study. The RESP is a relative measure for the similarity of a signal to the corresponding ground truth signal. The formal definition of the RESP can be found in Appendix B.

First, we analyze the RESP of the bus currents obtained from the simulations of the model (10) and the estimator (16). Figure 3 shows the three-phase average RESP of bus currents for model (10) and the estimator (16).
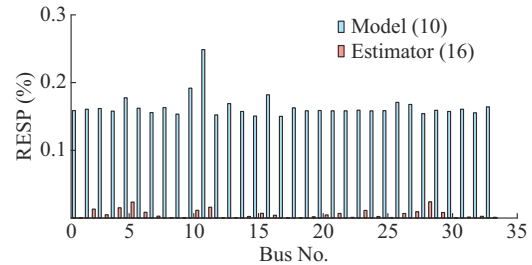
Fig. 3.   Three-phase average RESP of bus currents for model (10) and the estimator (16).

As can be observed, for each of the buses, the RESP of the model takes values equal to or less than 0.25%. Hence, the model (10) accurately reproduces the behavior of the ground truth model. The remaining differences between the models are due to numerical differences and can be further decreased by choosing a smaller simulation step size. For the estimator, we obtain even smaller RESP values of less than 0.025%. This is due to the measurement error feedback in an observer.

Figure 4 depicts the bus currents at bus 17 for the ground truth model, the model (10), and the estimator (16) for the time between 1.95 s and 2.10 s. We can clearly identify the system frequency of 50 Hz. Due to the load imbalance at phase B of bus 17, the amplitude of the current at phase B is slightly higher than those at the phases A and C. At $t = 2$ s, we see the load jump in which the amplitude of the bus current increases approximately by the factor of 2. As can be observed, the model (10) and the estimator (16) correctly reproduce the behavior of the ground truth model at this crucial point. Visually, we cannot distinguish between the obtained currents.

As an interim result, let us summarize that the model (10) accurately reflects the behavior of the ground truth model. Moreover, the estimator (16) produces the estimates that are very close to the values from the ground truth model.

Next, we compare the simulation results of the estimator (16) with the results obtained for a WLS estimator. For the estimator (16), the mean RESP over all reconstructed bus voltages is 0.0015% (standard deviation: 0.00092%). The respective value for the WLS estimator is 5.1% (standard deviation: 0.063%). Hence, the estimator (16) significantly outperforms the WLS estimator. This can be explained by two reasons. First, the WLS estimator cannot capture the harmon-

ic distortion. This is illustrated in Fig. 5 which shows one os-
cillation period of the voltage at phase A of bus 17 starting
from 2 s. In contrast to the WLS estimator, the estimator
(16) is able to reconstruct the harmonic distortion from the
ground truth model. Second, the WLS estimator cannot deal
with abrupt changes in the load. This is shown in Fig. 6
which depicts the estimated bus current for phase A of bus
17 between $t = 1.98$ s and 2.08 s. Here, the WLS estimator re-
quires about four periods to reach the amplitude of the cur-
rent computed by the estimator (16) and ground truth model.
Hence, as expected, on the sub-second time scale, the estima-
tor (16) significantly outperforms the WLS estimator, e.g., as
a basis for fast control and protection schemes.
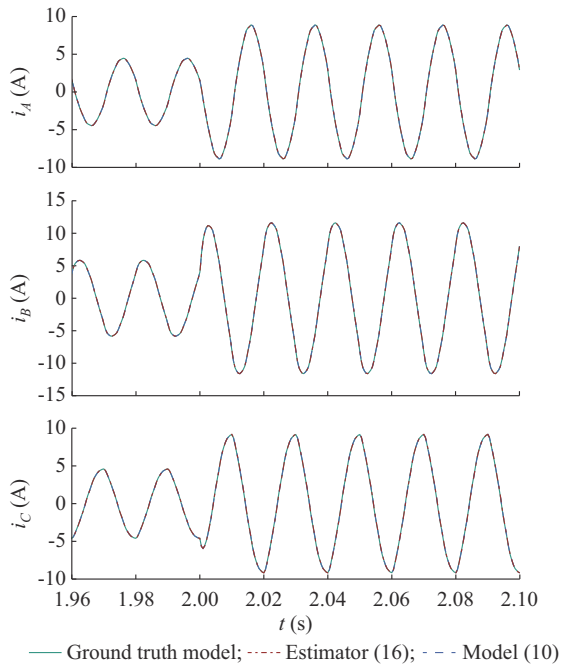
Fig. 4.   Bus currents at bus 17 for ground truth model, model (10) and es-
timator (16) for time between 1.95 s and 2.10 s.
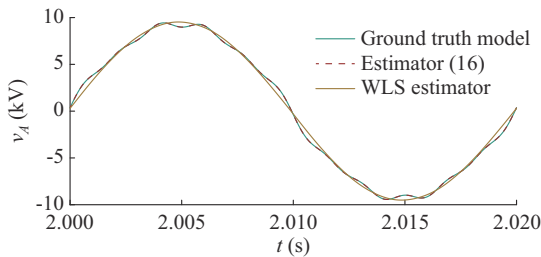
Fig. 5.   Bus voltages at phase A of bus 17 for ground truth model, estima-
tor (16), and WLS estimator for time between 2 s and 2.02 s.

In the last part of this case study, we now compare the re-
constructions from the estimator (16) and the WLS estimator
under measurement noise. To this end, the measurements
(13) are extended by noise, i.e., $\boldsymbol{m}_i = \boldsymbol{M}_i \boldsymbol{i}^{\mathrm{bus}} + \boldsymbol{\delta}$, where $\boldsymbol{\delta}$ is a
vector-valued Gaussian random process with zero mean and
covariance matrix $\sigma^2 \boldsymbol{I}_{\bar{q}}^2$, $\sigma \in \mathbb{R}_{\geq 0}$, where $\boldsymbol{I}_{\bar{q}}$ is the identity ma-
trix of order $\bar{q}$. The above simulations of the estimator (16)
and the WLS estimator are then repeated on the basis of the
noisy measurements.
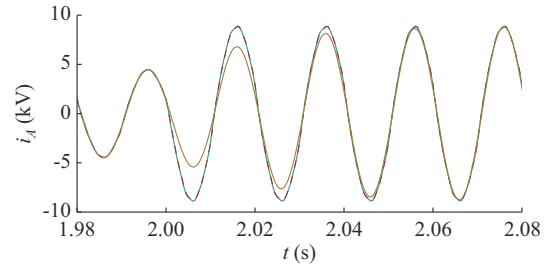
Fig. 6.   Bus currents at phase A of bus 17 for ground truth model, estima-
tor (16), and WLS estimator for time between 1.98 s and 2.08 s.

The results are depicted in Fig. 7. The figure shows the
mean RESPs of the reconstructed bus voltages for the esti-
mator (16) and the WLS estimator for different noise vari-
ances σ^2. For the six considered noise variances 10^{-5}, 10^{-4},
10^{-3}, 10^{-2}, 10^{-1}, and 10^{0}, the mean SNRs over all measure-
ment signals are given by 98.0 dB, 86.5 dB, 75.0 dB, 63.4
dB, 51.9 dB, and 40.4 dB, respectively. As can be observed,
starting at a low level, the mean RESP of the reconstructions
from the estimator (16) increases with increasing noise vari-
ance. In contrast, the RESPs of the WLS estimator are al-
most constant over the different noise variances. This can be
explained by the smoothing property of the PLLs for the
phasor computation in the WLS estimator.
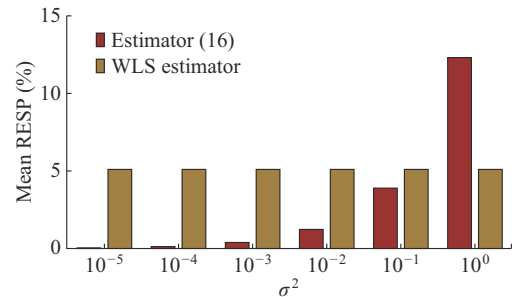
Fig. 7.   Mean RESPs over all voltages from reconstructions of estimator
(16) and WLS estimator for different noise variances σ^2.

Figure 7 shows that for a variance smaller than or equal
to 10^{-2} (i.e., an $SNR \geq 63.4$ dB), the estimator (16) gives ade-
quate reconstructions which have a significantly lower mean
RESP than the reconstructions obtained from the WLS esti-
mator. Note that the SNRs of sampled value measurements
from PMUs are considerably higher than 63.4 dB [26].
Therewith, for realistic SNR values, the estimator (16) out-
performs a WLS estimation. For low SNR values (e.g., from
low-quality measurement systems), however, we find a dete-
rioration of the reconstructions from the estimator (16),
which may be explained by the first time-derivative of the
current measurements in the estimator, as shown in (16c). In
such cases, however, we can still increase the SNR of the
measurements in a pre-processing using well-known noise
suppression methods from the field of low-pass and band-
pass filtering.

Finally, note that the 4 s simulation of the estimator (16)
is finished in about 2 s, which indicates its real-time capabil-
ity for a system of such size.

V. Conclusion

In this paper, we present an observer-based dynamic state estimator (i.e., (16)) for unbalanced three-phase power systems with synchronized sampled value measurements. The estimator is based on a PHS model (i.e., (10)), which explicitly considers the line dynamics. Our DSE can be designed offline in a fully automated manner (i.e., Algorithm 1). The estimator is able to capture sub-second phenomena such as transients from converter-based load and generation as well as harmonic distortion. Therewith, it extends the functionalities of a classical WLS-based power system state estimation towards modern control and protection schemes for converted-dominated systems. Future work will focus on a Kalman filter based approach to our state estimation in order to handle uncertainties.

Appendix A Strong* Detectability

The concept of strong* detectability extends the notion of detectability to systems with unknown inputs. Strong* detectability can be explained by the smoothing property of PLLs for phasor computation in WLS estimation. Here, we briefly recapitulate this concept.

Consider a linear state-space system $\boldsymbol{x} = \boldsymbol{Ax} + \boldsymbol{Bu}$, $\boldsymbol{y} = \boldsymbol{Cx} + \boldsymbol{Du}$ with initial state $\boldsymbol{x}|_{t=0} = \boldsymbol{x}_0$. The following definition is taken from [28].

Definition: the above system is strong* detectable if $\lim_{t \to \infty} \boldsymbol{y} \to$ *implies*, $\lim_{t \to \infty} \boldsymbol{x} \to \boldsymbol{0}$.

Appendix B Definition of RESP

Consider a ground truth signal $s_{\mathrm{gt}} \colon [0, T] \to \mathbb{R}$, $t \mapsto s_{\mathrm{gt}}(t)$. The mean power of the signal $s_{\mathrm{gt}}(t)$ is:

$$p_{\mathrm{gt}} = \frac{1}{T} \int_0^T s_{\mathrm{gt}}^2(t)\, \mathrm{d}t \tag{B1}$$

Furthermore, consider a second signal $s_{\mathrm{ap}}(t) \colon [0, T] \to \mathbb{R}$, $t \mapsto s_{\mathrm{ap}}(t)$ which represents an approximation of the signal $s_{\mathrm{gt}}(t)$. This approximation may stem from a model or an estimator. We define the error signal as $\varepsilon(t) s_{\mathrm{gt}}(t) - s_{\mathrm{ap}}(t)$. The mean error signal power is defined as:

$$p_{\varepsilon} := \frac{1}{T} \int_0^T \varepsilon(t)^2\, \mathrm{d}t = \frac{1}{T} \int_0^T \left(s_{\mathrm{gt}}(t) - s_{\mathrm{ap}}(t) \right)^2 \mathrm{d}t \tag{B2}$$

The RESP is defined as the quotient of (B2) and (B1):

$$r_{\varepsilon} := \frac{p_{\varepsilon}}{p_{\mathrm{gt}}} \tag{33}$$

References

[1] J. Zhao, A. Gomez-Exposito, M. Netto *et al.*, "Power system dynamic state estimation: motivations, definitions, methodologies and future work," *IEEE Transactions on Power Systems*, vol. 34, no. 4, pp. 3188-3198, Jul. 2019.

[2] M. Pfeifer, M. Zimmerlin, M. Schwarzendorfer *et al.*, "Weighted least squares state estimation for coupled power and gas distribution networks," in *Proceedings of 53rd IEEE International Universities Power Engineering Conference (UPEC)*, Glasgow, UK, Sept. 2018, pp. 1-8.

[3] F. C. Schweppe, "Power system static-state estimation, part III: implementation," *IEEE Transactions on Power Apparatus and Systems*, vol. 89, no. 1, pp. 130-135, Jan. 1970.

[4] A. S. Meliopoulos, G. J. Cokkinides, P. Myrda *et al.*, "Dynamic state estimation-based protection: status and promise," *IEEE Transactions on Power Delivery*, vol. 32, no. 1, pp. 320-330, Jan. 2016.

[5] North America Electric Reliability Corporation (NERC). (2016, Jan.). 1200 MW fault induced solar photovoltaic resource interruption disturbance report. [Online]. Available: https://www. nerc. com/pa/rrm/ea/1200_MW_Fault_Induced_Solar_Photovoltaic_Resource_/1200_MW_Fault_Induced_Solar_Photovoltaic_Resource_Interruption_Final.pdf.

[6] Z. Huang, H. Krishnaswami, G. Yuan *et al.*, "Ubiquitous power electronics in future power systems: recommendations to fully utilize fast control capabilities," *IEEE Electrification Magazine*, vol. 8, no. 3, pp. 18-27, Mar. 2020.

[7] Y. Liu, A. K. Singh, J. Zhao *et al.*, "Dynamic state estimation for power system control and protection," *IEEE Transactions on Power Systems*, vol. 36, no. 6, pp. 5909-5921, Nov. 2021.

[8] J. Zhao, M. Netto, Z. Huang *et al.*, "Roles of dynamic state estimation in power system modeling, monitoring and operation," *IEEE Transactions on Power Systems*, vol. 36, no. 3, pp. 2462-2472, May 2021.

[9] A. K. Singh and B. C. Pal, *Dynamic Estimation and Control of Power Systems*. London: Academic Press, 2019.

[10] H. H. Alhelou, M. E. H. Golshan, and N. D. Hatziargyriou, "Deterministic dynamic state estimation-based optimal LFC for interconnected power systems using unknown input observer," *IEEE Transactions on Smart Grid*, vol. 11, no. 2, pp. 1582-1592, Mar. 2020.

[11] G. Anagnostou, F. Boem, S. Kuenzel *et al.*, "Observer-based anomaly detection of synchronous generators for power systems monitoring," *IEEE Transactions on Power Systems*, vol. 33, no. 4, pp. 4228-4237, Jul. 2018.

[12] A. K. Singh and B. C. Pal, "Decentralized dynamic state estimation in power systems using unscented transformation," *IEEE Transactions on Power Systems*, vol. 29, no. 2, pp. 794-804, Mar. 2014.

[13] Y. Xiao, M. Lu, Z. Huang *et al.*, "Dynamic state estimation of power system considering asynchronous measurement," in *Proceedings of 2020 International Conference on Electrical Engineering and Control Technologies (CEECT)*, Melbourne, Australia, Dec. 2020, pp. 1-10.

[14] Y. Lee, S. H. Kim, G. Lee *et al.*, "Dynamic state estimation of generator using PMU data with unknown inputs," in *Proceedings of 2020 IEEE 29th International Symposium on Industrial Electronics (ISIE)*, Delft, Netherlands, Jun. 2020, pp. 1-9.

[15] G. Anagnostou and B. C. Pal, "Derivative-free Kalman filtering based approaches to dynamic state estimation for power systems with unknown inputs," *IEEE Transactions on Power Systems*, vol. 33, no. 1, pp. 116-130, Jan. 2018.

[16] J. Zhao, S. Wang, R. Huang *et al.*, "Robust adaptive decentralized dynamic state estimation with unknown control inputs using field PMU measurements," in *Proceedings of 2020 IEEE PES General Meeting (PESGM)*, Montreal, Canada, Aug. 2020, pp. 1-8.

[17] R. Xiao, G. Wang, X. Hao *et al.*, "Dynamic state estimation of medium-voltage DC integrated power system with pulse load," *Journal of Modern Power Systems and Clean Energy*, vol. 8, no. 4, pp. 689-698, Jul. 2020.

[18] N. Vieyra, P. Maya, and L. M. Castro, "Dynamic state estimation for microgrid structures," *Electric Power Components and Systems*, vol. 48, no. 3, pp. 320-332, Mar. 2020.

[19] L. Zhang, K. Lai, and M. S. Illindala, "Dynamic analysis and state estimation of a mixed energy source microgrid," in *Proceedings of 2020 IEEE Industry Applications Society Annual Meeting*, Detroit, USA, Oct. 2020, pp. 1-10.

[20] Y. Liu, A. Meliopoulos, L. Sun *et al.*, "Protection and control of microgrids using dynamic state estimation," *Protection and Control of Modern Power Systems*, vol. 3, no. 1, pp. 1-13, Jan. 2018.

[21] B. L. Nguyen, T. V. Vu, T. H. Ortmeyer *et al.*, "Distributed dynamic state estimation for microgrids," in *Proceedings of 2020 IEEE PES General Meeting (PESGM)*, Montréal, Canada, Aug. 2020, pp. 1-10.

[22] A. van der Schaft and D. Jeltsema, "Port-Hamiltonian systems theory: an introductory overview," *Foundations and Trends in Systems and Control*, vol. 1, no. 2, pp. 173-378, Feb. 2014.

[23] M. E. Baran and F. F. Wu, "Network reconfiguration in distribution systems for loss reduction and load balancing," *IEEE Power Engineering Review*, vol. 9, no. 4, pp. 1401-1407, Apr. 1989.

[24] W. H. Kersting, *Distribution System Modeling and Analysis*. Boca Raton: Taylor & Francis, 2017.

[25] S. Boyd and L. Vandenberghe, *Introduction to Applied Linear Algebra*. Cambridge: Cambridge University Press, 2018.

[26] A. G. Phadke and J. S. Thorp, *Synchronized Phasor Measurements and Their Applications*. Cham: Springer, 2017.

[27] M. Darouach, M. Zasadzinski, and S. Xu, "Full-order observers for lin-

ear systems with unknown inputs," *IEEE Transactions on Automatic Control*, vol. 39, no. 3, pp. 606-609, Mar. 1994.

[28] M. L. J. Hautus, "Strong detectability and observers," *Linear Algebra and its Applications*, vol. 50, p. 356, 1983.

[29] M. Hou and R. J. Patton, "Input observability and input reconstruction," *Automatica*, vol. 34, no. 6, pp. 789-794, Jun. 1997.

[30] J. Y. Wong. (2021, Oct.). IEEE 33 bus system. [Online]. Available: https://www. mathworks. com/matlabcentral/fileexchange/73127-ieee-33-bus-system

[31] *Recommended practice and requirements for harmonic control in electric power systems*, IEEE Std 519-2014.

[32] S. Golestan, M. Ramezani, J. M. Guerrero *et al*., "Moving average filter based phase-locked loops: performance analysis and design guidelines," *IEEE Transactions on Power Electronics*, vol. 29, no. 6, pp. 2750-2763, Jun. 2014.

Martin Pfeifer received the B. Sc., M. Sc., and Ph. D. degrees in electrical engineering and information technology in 2012, 2014, and 2021, respectively, from the Karlsruhe Institute of Technology (KIT), Karlsruhe, Germany. Currently, he is the Head of the research group networked multi-energy systems at the Institute of Control Systems (IRS) at KIT. His main research interests include physical and data-based methods for modeling and supervision of multi-energy systems.

Felicitas Mueller received the B. Sc. and M. Sc. degrees in electrical engineering and information technology, in 2015 and 2018, respectively, from the Karlsruhe Institute of Technology (KIT), Karlsruhe, Germany. She is pursuing the Ph.D. degree as a Research Assistant at the Institute of Electrical Energy Systems and High Voltage Technology (IEH) at KIT. Her research interests include sector-coupling and optimization of multi-energy systems.

Steven de Jongh received the B. Sc. and M. Sc. degrees in electrical engi-neering and information technology, in 2015 and 2018, respectively, from the Karlsruhe Institute of Technology (KIT), Karlsruhe, Germany. Currently, he is pursuing the Ph.D. degree as a Research Assistant at the Institute of Electrical Energy Systems and High Voltage Technology (IEH) at KIT. His research interests include machine learning algorithms applied in power system estimation and optimization.

Frederik Gielnik received the B. Sc. and M. Sc. degrees in electrical engineering and information technology, in 2016 and 2019, respectively, from the Karlsruhe Institute of Technology (KIT), Karlsruhe, Germany. He is pursuing the Ph.D. degree as a Research Assistant at the Institute of Electrical Energy Systems and High Voltage Technology (IEH) at KIT. His research interests include dynamic modeling and optimization of power systems.

Thomas Leibfried received the Dipl. -Ing. and Dr. -Ing. degrees from the University of Stuttgart, Stuttgart, Germany, in 1990 and 1996, respectively. From 1996 to 2002, he was with Siemens AG, Nuremberg, Germany, working in the power transformer business in various technical and management positions. In 2002, he joined the University of Karlsruhe, Karlsruhe, Germany, as the Head of the Institute of Electric Energy Systems and High-Voltage Technology (IEH). He is a member of VDE and CIGRE. His research interests include power and energy networks.

Sören Hohmann studied the electrical engineering at the Technische Universität Braunschweig, University of Karlsruhe and école nationale supérieure d'électricité et de mécanique Nancy. He received the diploma degree and Ph.D. degree from the University of Karlsruhe, Karlsruhe, Germany, in 1997 and 2002, respectively. Afterwards, until 2010, he worked in the industry for BMW, Munich, Germany. Today, he is the head of the Institute of Control Systems (IRS) at the Karlsruhe Institute of Technology (KIT), Karlsruhe, Germany, as well as a Directors Board Member of the Research Center for Information Technology (FZI), Karlsruhe, Germany. His research interests include cooperative control, multi-energy systems.